Competitive Interactions at Electrolyte/Octanol Interfaces—A Molecular Perspective

Nitesh Kumar,[*,†] Michael J. Servis,[†] Zhu Liu,[†] and Aurora E. Clark[*,†,‡]

†*Department of Chemistry, Washington State University, Pullman, Washington 99164*

‡*Pacific Northwest National Laboratory, Richland, Washington 99354*

E-mail: nitesh.kumar@wsu.edu; auclark@wsu.edu

Abstract

Much is understood about electrolyte liquid/liquid interfaces, yet the relationships between ion solvation, adsorption, and the instantaneous surface have not been the topic of significant study. The thermally corrugated capillary wave characteristics of the instantaneous aqueous surface contribute to heterogeneous interfacial structural and dynamic properties. Those properties are sensitive the nature of the immiscible nonpolar solvent. In this work, we examine the role of interfacial heterogeneity upon ion behavior and further, how this is influenced by a partially polar solvent relative to a vapor phase analog. We compare and contrast ion solvation in electrolyte/vapor and electrolyte/octanol biphasic systems, focusing upon the changes to interfacial heterogeneity in the presence of the octanol solvent and the variations of ion concentration at different interfacial regions. The interplay between competing forces introduced by strong octanol water interactions at the interface is examined, with a new understanding of how such competition may lead to tailored interfacial properties.

Introduction

Aqueous electrolyte interfaces (with either a vapor phase or an immiscible liquid), have been a topic of significant research for the last two decades.[1–3] Although advances in instrumentation have enabled some spectroscopic characterization,[4–6] simulation using statistical mechanics methods, notably molecular dynamics (MD), has been an essential complement to our current understanding of liquid interfacial chemistry.[7–9] The molecular-level asymmetry of the interface has significant consequences for ion behavior and relative energetic preference for the interfacial region. Generally, "interfacial ion adsorption" implies that there is

a free energy minima for ions to exist within the interfacial region; this often causes an excess or increase in ion concentration relative to the bulk. Similarly, an ion concentration in the interface that is the same as in the bulk implies no changes to the free energy of the ion as it approaches the interface, while depletion of ion concentration indicates a decrease in energetic favorability for the ion to reside in this region. The change in ion solvation environment is a major factor that dictates these energetic preferences. For example, at the electrolyte/vapor interface, the general loss of H_2O hydrogen bonds (HBs) causes competition between these interactions and ion solvation, and can lead to a loss of solvating H_2O for the ion that thermodynamically disfavors interfacial adsorption.[10–12] If the ion has a large enough hydration energy, then ion solvation can be retained via restructuring of the interfacial H-bonding network.[13–15] At the same time, the orientational order of water induces an electrostatic potential difference between the liquid and vapor phases that, in turn, interacts with the ion charge density.[12] In general, small nonpolarizable ions respond more weakly to the interfacial electric field, whereas large and polarizable ions can have a favorable interaction that support adsorption. Many of the features of electrolyte/vapor interfaces carry over to that of electrolyte/liquid interfaces, where the liquid is a non-polar solvent.

The characterization of interfacial structure generally falls into two categories based upon whether the average perturbations to solvent interactions are considered over a 1-2 nm region of the interface or whether the instantaneous surface (and its subjacent layers) is explicitly examined. The instantaneous, as opposed to time average, surface accounts for the thermally corrugated nature of the interface as well as its capillary wave characteristics. Understanding the instantaneous surface is absolutely essential to a wide variety of interfacial properties, including the protrusions of solvent that can form during transport of solutes across the liquid liquid phase boundary.[16,17] Although much progress has been made in the analysis of the instantaneous surface for water/vapor and water/liquid interfaces, time averaged properties are still typically considered. Yet the instantaneous surface can be highly heterogeneous in both its structural organization and dynamic properties. Significant differences between

crest vs. trough regions may impact interfacial reactivity.[10,16] Based upon the "bulk-like" HB structure of the troughs of the water/vapor interface versus the "gas-like" water in the crests, one may anticipate partitioning of ion concentration between these distinct regions. At the same time, the local orientation for water is quite different in these regimes, which may also influence the local interfacial electric field.

Ion perturbation of interfacial characteristics has generally been broached only in the context of interfacial tension, γ, and molecular density distributions, but is closely related to the ongoing and controversial topic of whether ion adsorption enhances or diminishes capillary wave fluctuations, or interfacial roughness. Initial work implied that ions at the interface "pin" capillary waves and decrease the interfacial area of the surface,[18,19] whereas more recent work surmised that the original conclusion derived from finite size effects of the interfacial area and that in fact interfacial ions enhances capillary wave fluctuations.[20] The manner in which surface roughness influences the distribution of ions in the interfacial region is relatively unexplored, and the extension of this line of enquiry to amphiphilic solvents has not been performed. The direct interaction of an immiscible polar solvent with interfacial aqueous ions presents an intriguing contrast to the electrolyte/vapor case, as polar solvents may impart their own organizational features and introduce new competitive interactions. Toward this end, this work compares the behavior of ions in electrolyte/vapor and electrolyte/octanol biphasic systems. Two interfacial regions are investigated: 1) slabs that contain crest and troughs of the instantaneous surface as well as several subjacent layers, and 2) the instantaneous surfaces themselves of the electrolyte or octanol. We examine the changes to crest and trough regions in the water/octanol and electrolyte/octanol systems relative to their vapor analogs, and investigate the concentration of ions within different interfacial regions. When the instantaneous surface exhibits significant interfacial heterogeneity, ions are observed almost exclusively in "trough" regions. However, octanol creates a highly interdigitated instantaneous surface with that of water which decreases the variation between crest and trough hydrogen bond networks. Thus, ion concentration at

electrolyte/octanol interfaces increases relative to the analogous vapor phase, not because octanol helps to solvate the ions, but rather because the strong water-octanol interactions decrease the ion's tendency to lose waters of solvation in the interfacial region. This interplay of competing forces introduced by strong octanol-water interactions provides one mechanism for altering ion concentration and potentially reactivity at the interface.

Computational Methods

Simulation Protocol and Force Field Benchmarking

All simulations were performed using the GROMACS 2016.2[21] software package using periodic boundary conditions. Classical MD simulations of the 1M electrolyte/vapor systems ($NaNO_{3(aq)}$ or $CsNO_{3(aq)}$) were performed with 7205 H_2O and 130 $NaNO_3$ or $CsNO_3$ ions, respectively, and a unit cell of size 60×60×180 Å (Figure S1 in Supplementary Information). The initial system configurations were generated by randomly distributing molecules in adjacent phases using Packmol,[22] with ions placed in the aqueous phase. After energy minimization, the electrolyte/vapor system evolved in the NVT ensemble, using a 2 fs timestep, at 300 K for 20 ns of equilibration, followed by 40 ns used for data analysis. Analogous liquid/liquid interface simulations of water/octanol, $NaNO_{3(aq)}$/octanol and $CsNO_{3(aq)}$/octanol consisted of 2470 octanol molecules and 7205 water containing 130 $NaNO_3$ or $CsNO_3$ ions in 60×60×240 Å simulation boxes. The water/octanol systems were equilibrated for 40 ns in NPT and NVT respectively, followed by 40 ns of production run in NVT (Table S1). Nose-Hoover thermostat and Parrinello-Rahman barostat were used for temperature and pressure coupling respectively. Finite size effects were examined as described in the Supplementary Information.

Extensive force field benchmarking was performed, with details provided in the Supplementary Information and briefly summarized here. All simulations employed with a 1.6 Å cutoff for both short range electrostatic and van der Waals interactions. Particle-Mesh Ewald

summation[23] was used to treat long range electrostatics. The TIP3P model[24] was employed for water. The Na^+ and Cs^+ ions were modeled using the force fields of Joung *et al.*[25] Bulk $NaNO_3$ simulations were performed at a concentration of 1.875 M to benchmark the force fields to experimental data[26] (radial distribution functions (RDFs) presented in Figure S2), which resulted in an average aqueous phase bulk Na^+-H_2O solvation coordination number (CN) of 5.38 under a 3.20 Å Na^+-O_{H_2O} cutoff, in good agreement with prior work.[27,28] In the case of Cs^+, a CN of 8.80 H_2O is observed under a 4.10 Å Cs^+-O_{H_2O} cutoff in the bulk aqueous phase, also agreeing with prior AIMD studies.[29] Two different nitrate force fields were tested: those of Wipff *et al.*[30,31] and Papoyan. *et al.*[32] The Wipff *et al.*[30] force field was chosen for all data reported in this work because it best represented the experimentally observed Na^+...NO_3^- and NO_3^-...H_2O RDFs,[26,33] where on average 2 solvating H_2O are observed per nitrate O_N to yield a total of six solvating H_2O about NO_3^- (Figure S2).

The Joung and Wipff ion force fields were tested for their ability to reproduce the electrolyte/vapor interfacial properties, where the SPC/E, TIP3P and TIP4P-ew[34,35] water models were considered. The interfacial tension for pure TIP3P water/vapor was calculated as 48.71 mN/m, in good agreement to the literature value of 49.20 mN/m (Figure S3).[36,37] In the case of the electrolyte/octanol and water/octanol systems, the TIP3P water model with the OPLS force field parameters for octanol and charges.[38] All employed force fields are presented in Tables S2-S4.

Data analysis

Interfacial Tension. The interfacial tension, γ, was calculated using the pressure tensor method[39] as an integral over the z dimension with a box length L_z as

$$\gamma = \frac{1}{N_{int}} \int_0^{L_z} \frac{1}{2} \langle P_{zz} - \frac{1}{2}(P_{xx} + P_{yy}) \rangle dz, \quad (1)$$

where N_{int} is the number of interfaces (Figure S1) and P_{zz}, P_{yy}, and P_{xx} are the diagonal components of the pressure tensor.

Orientation Profiles of Water and Octanol. The time average dipole vector orientation for H_2O was calculated in 1 Å slabs in the z direction using

$$\left\langle \cos(\theta_i) \right\rangle = \left\langle \sum_i \hat{\mu}_i \cdot \hat{n}_z \right\rangle, \tag{2}$$

where $\cos(\theta_i)$ is the angle between the unit dipole vector and the z axis perpendicular to the interface. The unit dipole vector, $\hat{\mu}_i$, of water molecule i is dotted with the unit vector normal to interfacial plane, $\hat{n}_z$, pointing along z direction. The molecular orientation of octanol was calculated the same way, but instead using the unit vector passing through the terminal C-atom and the O-atom, as in prior work.[40,41]

Instantaneous Interface. The "Identification of Truly Interfacial Molecules (ITIM)" algorithm[42,43] was used to identify the instantaneous interfacial molecules of H_2O and octanol, employing the recommended probe sphere of radius 1.5 Å and a grid spacing of 0.2 Å. In the case of water, four subjacent layers were also identified. The interfacial width of water, d, was calculated as the full width at half maximum (FWHM) of the density profile of the H_2O center of mass instantaneous surface layer, fitted to a probability density function having a Gaussian distribution.

Crest and Trough Regions of the Interface. The interfacial crest and trough regions were identified from the density profile of the truly interfacial H_2O molecules and combined with a slab analysis to determine the H_2O and ions present in all crest and trough containing regions. Two slabs of 0.5×FWHM were created on either side of the mean μ of the instantaneous surface layer, with the slab towards the aqueous phase containing all interfacial trough molecules/ions and that towards organic phase containing the interfacial crest (see Figure S4).

Topological Data Analysis of Intermolecular Interactions. Networks of H_2O...H_2O, H_2O...ion,

H_2O...Oct, ion...Oct interactions were analyzed using the ChemNetworks program.[44] Hydrogen bonds were defined with an O...H distance cut-off based upon the first minimum of the O...H RDF (Table S5) and an O...H-O angle of 145-180°. Ion interactions were defined solely with a distance cutoff based upon the first minimum of the RDFs as given in Supplementary Information.

Residence Time within the Interfacial Region. The survival probability *L(t)* of ions and H_2O to be present in interfacial crest and trough regions, was determined by the correlation function of the ion being present at times t and $t+\delta t$. The computed probability *L(t)* at time t was fitted to an exponential function of form

$$\mathrm{L(t)} = \mathrm{a}_1 e^{-(\frac{\mathrm{t}}{\tau_1})^{\beta_1}} + \mathrm{a}_2 e^{-(\frac{\mathrm{t}}{\tau_2})^{\beta_2}}, \tag{3}$$

where τ_1 and τ_2 represent the residence times with contributions given by a_1 and a_2 respectively for each exponential terms. The fitting parameters β_1 and β_2 are called stretched exponents,[45] that are generally used for the calculation of residence times of species in heterogeneous systems.[46] The net residence time τ is

$$\tau = \mathrm{a}_1\tau_1 + \mathrm{a}_2\tau_2. \tag{4}$$

Analysis of the Willard-Chandler Surface. The interfacial surface area of all systems was determined using a procedure of continuous representation of a discrete instantaneous configuration of surface waters proposed by Willard and Chandler.[47,48] This procedure provides a reliable definition of the relevant spatial fluctuations in space and time of the interface location, which is otherwise averaged out by using the Gibbs dividing surface. We adopt the suggested coarse-graining length 2.5 Å and 90% water bulk density criterion in obtaining the Willard-Chandler surface of water. Ensemble average values of the interfacial area are obtained by averaging the individual areas of the instantaneous Willard-Chandler interfaces for each system. The normalised change in interface area, ΔA, is measured relative to a flat

surface having the same xy dimension as,

$$\Delta A = \langle A(WC) - A \rangle, \tag{5}$$

where A(WC) is the area of Willard-Chandler surface, A is the area of flat surface (xy Å). The range of z for different systems is the width of Gaussian distribution of interfacial water density as shown in Figure 1A & B. ΔG_{def} is defined as the average free energy required to perturb a flat interface to an interface with capillary wave structure.[49,50] It is defined by by[19]

$$\Delta G_{def} \approx \gamma \times \Delta A, \tag{6}$$

where γ is the interfacial tension.

Results and Discussion

We first present a brief but detailed description of the characteristics of the instantaneous surface for the water/vapor and water/octanol systems. These data illustrate the impact of strong H_2O...Oct interactions upon organizational structure. Then, we study the partitioning of ion concentration in crest vs. trough regions. The variations in ion behavior due to specific ion effects are also discussed. Finally, we determine how the presence of ions influences the instantaneous surface of water.

Heterogeneity of water/vapor vs. water/octanol interfaces

Prior study has examined the water/vapor interface and the distribution of H-bonding environments that occur in crests vs. troughs of the instantaneous surface.[10,51] Although water/octanol interfaces have been the topic of much research, the primary emphasis has been upon understanding the spatial average of interfacial properties across the rough surface. The experimental interfacial tension, γ, is an order of magnitude smaller for the neat

water/octanol (8.52 mN/m) relative to water/vapor (71.73 mN/m),[36,52] a trend reproduced by our simulations—although the interfacial tension of TIP3P-water/vapor is notoriously difficult to match to experiment (Table 1).[36,53] Interestingly, both the interfacial width, d, and interfacial area, ΔA, decrease despite the decrease in interfacial tension of water/octanol relative to water/vapor (Table 1). If the interfacial width is representative of a commensurate change in interfacial area, then the water/octanol system deviates from the relationship of γ with the mean curvature (capillary wave behavior) via the Young-Laplace equation[54]. One possibility for this behavior may be that there is a larger difference than normal between length scales of the local thermal fluctuation and capillary wave oscillations, caused by significant coupling of interactions between octanol and water.

In part, these data support potential dampening of the capillary wave fluctuations in water/octanol interface relative to water/vapor, a feature further pursued by studying changes to the organization of crest vs. trough regions. As previously noted for water/vapor,[10] there is a loss of ∼0.4-0.5 H_2O...H_2O H-bonds in the crest region that projects into the vapor phase relative to the trough region that projects into the water bulk (Table 1). In the water/octanol system, this value is within statistical uncertainty, though there may be a small decrease in the variation given that a similar decrease is observed using the TIP4P-ew water model and the GROMOS force field[55] for octanol, as demonstrated in Figure S11. Instead, the variation in dipole orientations in crest vs. trough is significantly subdued in water/octanol relative to water/vapor. The variations in dipole orientations in crest versus trough regions has been discussed,[10] and in the case of water/vapor and water/hexane, the water in the trough (closer to the water bulk) have their dipole orientated towards the water phase, whereas those in the crest have their dipole pointing out of the water phase (Figure 1A). Yet in the water/octanol case, the water dipole orients toward the water bulk phase irrespective of where those interfacial waters reside.

Table 1: Average values of interfacial tension (γ), interfacial width (d), and average increase in normalized interfacial surface area (ΔA) per Willard-Chandler interface of water, corresponding free energy of deformation (ΔG_{def}). The surface tension convergences are given in Figures S11 & S12. The average number of H_2O...H_2O H-bonds present in the crest- and trough-containing slabs and the bulk aqueous region are also presented with statistical uncertainties. Note that 'exp' stands for experimental.

System	γ (mN/m)	d(Å)	ΔA (Å^2)	ΔG_{def} (kJ/mol)	H-bond Crest	H-bond Trough	H-bond Bulk
Water/vapor(exp)[36]	71.73	—	—	—	—	—	—
Water(TIP3P)/vapor	48.71	4.68	585.44	285.17	2.27±0.07	2.67±0.01	2.83±0.03
1M $NaNO_{3(aq)}$/vapor	50.42	4.59	572.08	288.44	2.38±0.08	2.69±0.09	2.69±0.04
1M $CsNO_{3(aq)}$/vapor	49.33	4.66	571.70	282.02	2.36±0.04	2.67±0.02	2.69±0.04
Water/octanol (exp)[52]	8.52	—	—	—	—	—	—
Water(TIP3P)/octanol	14.21	4.15	405.16	57.57	2.34±0.08	2.52±0.06	2.92±0.01
1M $NaNO_{3(aq)}$/octanol	32.15	4.22	477.80	153.61	2.01±0.04	2.48±0.01	2.67±0.09
1M $CsNO_{3(aq)}$/octonol	20.74	4.31	468.69	97.21	2.04±0.07	2.52±0.08	2.73±0.09

In combination, these data indicate that the water/octanol interface has less variation in crest vs. trough characteristics relative to water/vapor. Two different arrangements of the instantaneous surfaces of water and octanol could lead to this result. First, is that the water and octanol ITIM layers are flattened and laying essentially "on top of" each other with minimal surface roughness. In this case, one would expect that the density profile of the ITIM layers would be offset by a distance larger than 2× the 1.6 Å atomic radius of O-atom. Instead, the peak of the octanol distribution is only 0.4 Å offset from that of water (Figure 1B, using the center of mass of H_2O). A second option is that the surface layers of H_2O and octanol become "interdigitated" where individual octanol -OH groups and H_2O have overlapping density in the z direction. This is indicated by the density profiles in Figure 1B, the analysis of HB patterns, and the 2-dimensional Oct...Oct RDF. The most likely H-bonding configuration of octanol derives from each octanol having 1 H-bond with water and 2 H-bond with other octanol. Such species are present in water-bridged octanol dimers, that emerge in the broad peak at 4.21 Å in the 2D Oct...Oct RDF (Figure 1D). The strong water-octanol interaction is further supported by a decrease in H_2O residence times, τ, when in the water/octanol relative to water/vapor. In the water/vapor case, the dangling -OH causes much stronger H_2O...H_2O interactions and leads to a τ of 43 ps. This value decreases to 23 ps in water/octanol as the octanol minimizes loss of H_2O HB's as it becomes a part of the HB network at the interface. Each of these features futher supports the observation that the free energy of interface deformation ΔG_{def} decreases nearly fourfold in the water/octanol interface.

In summary, in the electrolyte free systems it is observed that the water/octanol interface significantly has less variations in the local structure of crest and trough regions of the instantaneous surface than the corresponding water/vapor interface. This is due to strong water/octanol interactions and the subsequent "interdigitation" of water and octanol in the interfacial layer.

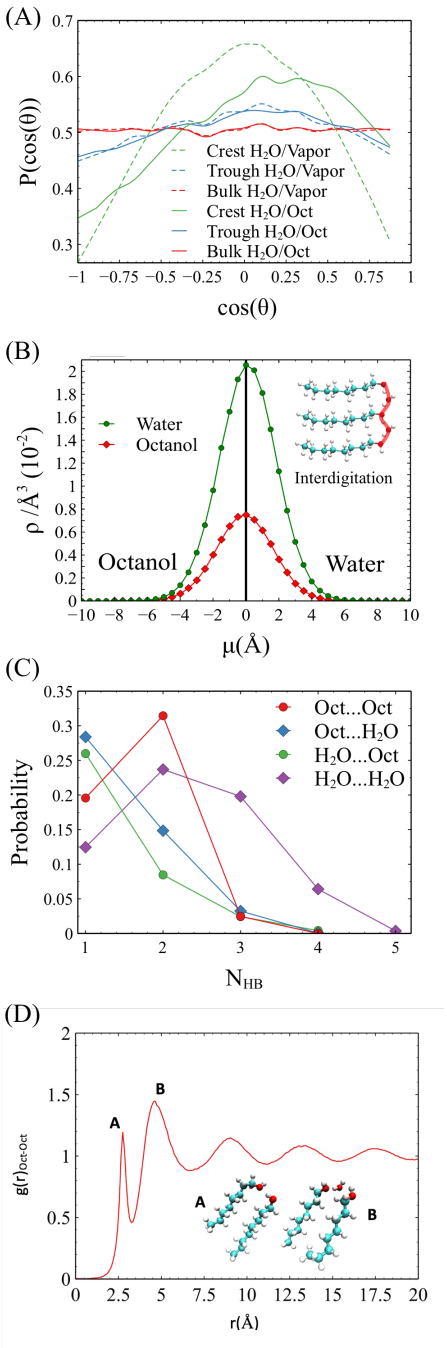

Figure 1: (A) Comparison of the H_2O dipole orientation (Equation 2) in water/vapor and water/octanol. (B) Number-density distribution of the truly interfacial layer of H_2O and octanol. (C) The HB distribution of octanol and water in truly interfacial layer, where the probability of H_2O...Oct and H_2O...H_2O interactions is normalized to 1 as is the Oct...Oct and Oct..H_2O interactions. (D) 2D RDF of octanol molecules present in the truly interfacial layer. The probability distribution of octanol molecules corresponding to the interfacial configurations are shown in the inset.

Ion Behavior Influenced by Surface Roughness

It is well-known that the presence of ions at aqueous/nonpolar interfaces generally increases the interfacial tension, γ and decreases interfacial width, d.[3,4,51,56–59] Specific ion effects are also observed (in this work and others), where small cations like Na^+ decrease d (and increase interfacial tension) more strongly than larger ions like Cs^+.[60,61] Although these observations are well-known for electrolyte/vapor and interfaces with non-polar solvents, the outcome in the presence of a polar immiscible solvent is not well studied. In this case, we examine the impact of competetive H_2O...Oct, ion...H_2O and ion...Oct interactions upon interfacial structure and macroscopic properties.

The density profiles of the cations, anions and corresponding H_2O across the interfacial region is presented in Figure S5. Yet more interesting is the partitioning of the ions within the crest and trough regions and the comparison of their behavior in the vapor and octanol systems. Toward this aim, we calculated the average percent of ions in the simulation that are observed within the truly interfacial layer and subjacent layers (Table 2). Considering first electrolyte/vapor, the ion density profile agrees with prior studies[3,3,12,62] where, due to the size and polarizability of the NO_3^- anion, an interfacial anion excess is observed relative to the cation. The ratio of cations to anions in the truly interfacial layer is $\sim$1:4 at the $NaNO_{3(aq)}$/vapor interface and $\sim$1:2 at the $CsNO_{3(aq)}$/vapor interface. Thus, between the two cations, there are more Cs^+ relative to Na^+, as anticipated by their relative size, polarizability, and hydration free energies.[63–65]

The Gibbs dividing surface is generally used as a reference for the interfacial region, often based on the position where the density of water is half of the bulk. In contrast, we define "crest" and "trough" regions of the instantaneous surface using the peak of the ITIM water distribution as the midpoint of the surface, defined as $\mu = 0$. The ion concentration in crest and trough regions is illustrated by the number density in the truly interfacial layer as a function of μ (Figure 2A). In this case, ion density in negative μ regions of the green ITIM water curve indicate ion concentration within the crest part of capillary waves (or ions

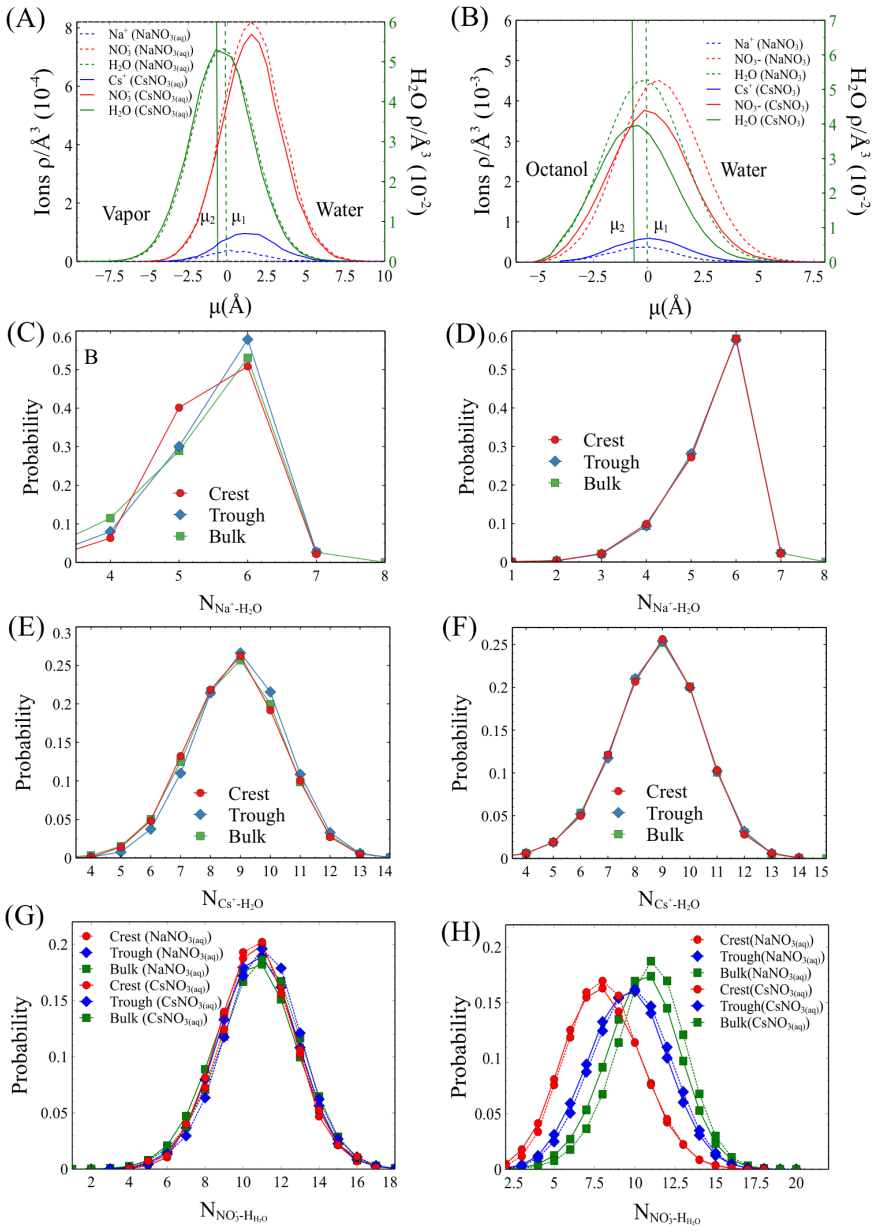

Figure 2: (A) Number density of H_2O and ions within the truly interfacial layer of $NaNO_{3(aq)}$ and $CsNO_{3(aq)}$ vapor interfaces. (B) Number density of H_2O and ions within the truly interfacial layer at $NaNO_{3(aq)}$ and $CsNO_{3(aq)}$ octanol interfaces.(C) The number of H_2O solvating Na^+ present in the interfacial regions of $NaNO_{3(aq)}$/vapor. (D) The number of H_2O solvating Na^+ present in the interfacial regions of $NaNO_{3(aq)}$/octanol. (E) The number of H_2O solvating Cs^+ ions present in the interfacial regions of $CsNO_{3(aq)}$/vapor. (F) The number of H_2O solvating Cs^+ ions present in the interfacial regions of $CsNO_{3(aq)}$/octanol. (G) The number of H_2O solvating $O_{Nitrate}$ of NO_3^- ions present in the interfacial regions of $ions_{(aq)}$/vapor. (H) The number of H_2O solvating $O_{Nitrate}$ of NO_3^- ions present in the interfacial regions of electrolyte/octanol.

Table 2: The percent distribution of electrolytes in various interfacial layers in both electrolyte/vapor and electrolyte/octanol systems.

Interfacial Layer	Na^+($NaNO_3$)	NO_3^-($NaNO_3$)	Cs^+($CsNO_3$)	NO_3^-($CsNO_3$)
water/vapor				
1	0.3± 0.6	2.2±0.9	1.0±0.1	2.0±0.7
2	5.6±0.4	8.6±0.3	8.0±0.6	7.7±0.8
3	10.3±0.1	10.9±0.7	10.6±0.4	10.3±0.2
4	11.4±0.9	11.8±0.1	11.5±0.7	11.3±0.9
5	11.9±0.4	11.8±0.7	11.8±0.9	11.7±0.8
water/octanol				
1	3.0±0.8	11.5±0.3	6.9±0.2	12.3±0.8
2	10.0±0.5	8.4±0.6	11.5±0.3	8.4±0.6
3	10.0±0.5	9.2±0.3	10.0±0.6	9.2±0.3
4	10.0±0.6	9.2±0.3	9.2±0.3	9.2±0.3
5	10.0±0.5	9.2±0.3	9.2±0.3	9.2±0.3

that are solvated by crest H_2O) and density in the positive μ region represents ions within troughs that point to the aqueous phase (or ions that are solvated by trough containing H_2O). Importantly, all ion types are preferentially observed in the trough region of the rough surface. This preference is nearly identical irrespective of whether the electrolyte is $CsNO_3$ or $NaNO_3$, even though the interfacial Cs^+ concentration is higher than that of Na^+. As previously described for the pure water/vapor interface, the trough regions have water H-bonding and orientation characteristics that are nearly the same as the bulk phase, and thus ions that reside in the trough minimize loss of H_2O...H_2O hydrogen bonding and/or the ion waters of solvation, as the H_2O CN are nearly identical for trough-residing cations and those in the bulk phase (Figures 2C-E). In contrast, those small numbers of ions that reside in the crest region lose solvating waters. This is most pronounced for the Na^+, and observed to a lesser extent for Cs^+ and $NO_3{}^-$.

Significant differences in these behaviors emerge when considering the water/octanol surface. First, a 10× increase in Na^+ and $NO_3{}^-$ concentration is observed in the truly interfacial layer relative to the vapor interface, while Cs^+ exhibits an $\sim 7\times$ increase (Table 2). All ions are still preferentially observed in regions of the rough surface that protrude into the aqueous phase, yet comparison of Figures 2A-B illustrates that the ion distribution at the

electrolyte/octanol interface overlaps more with the water ITIM distribution in the octanol interface because there is less variation in the characteristics between crest and trough regions in the electrolyte/octanol system relative to the electrolyte/vapor. As observed in Figure 2D and 2F, cations at the electrolyte/octanol interface have, on average, the same number of solvating waters as the bulk, and irrespective of whether they are reside in a nominally crest vs. trough region.

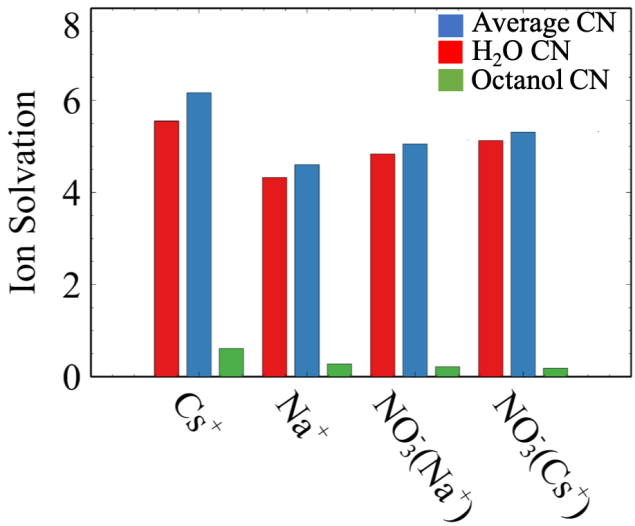

Figure 3: The distribution of solvation coordination number (CN) of all interfacial ions.

Within the truly interfacial layer of water, competition of the H_2O...ion, Oct...ion, Oct...H_2O and H_2O...Oct interactions may have an important impact upon the ion solvation. Further, changes to ion concentration at the interface has the potential to lead to different concentrations of ion paired species. To understand the interfacial ion...Oct interactions, we plotted the average number of interactions in Figure 3. On average, the Na^+ ions are solvated by 0.27±0.08 octanol molecules and Cs^+ by 0.61±0.02 octanol molecules. The average nitrate solvation by interfacial octanol is significantly less than that for the cations, at 0.18±0.05 for $NaNO_{3(aq)}$ and 0.21±0.07 for $CsNO_{3(aq)}$. This result indicates that within the competition of between Oct...ion and Oct...H_2O interactions, the octanol is more effectively able to interact with H_2O and maximize those interactions as opposed to participating in partial solvation with the ions of the electrolyte. Contact ion pairs were found to be rare in both

electrolyte/vapor and electrolyte/octanol systems (Figure S6). In combination, these data indicate that the increase of ion concentration at the electrolyte/octanol interfaces relative to the vapor phase occurs because the strong water-octanol interactions decrease the ion's tendency to lose waters of solvation in the interfacial region.

Dynamic Aspects of Interfacial Ions

The residence time, τ, of water in the interfacial slabs decreases dramatically in the electrolyte systems[66] relative to the pure solvent biphasic systems. Moving from water/vapor to $NaNO_{3(aq)}$ the H_2O τ decreases from 43 to 9.9 ps, and is calculated to be 14 ps in $CsNO_{3(aq)}$. Similar behavior is observed when comparing the residence time of H_2O in going from water/octanol (23 ps) to $NaNO_{3(aq)}$/octanol (4.5 ps) and $CsNO_{3(aq)}$/octanol (2 ps). Ion dynamics in the crest and trough slabs are ion specific, where Na^+ ions prefer to reside longer in the interfacial region of electrolyte/vapor compared to electrolyte/octanol whereas reverse trend is observed for Cs^+ ions. In general, ions prefer to reside longer in the trough region compared to crest. The average residence time of Cs^+ at the octanol interface was found to be 700 ps compared to 4 ps for Na^+. We also observed a longer residence time for NO_3^- ions in the system of $CsNO_3$ at both vapor and octanol interfaces. The increased net positive charge density from the Cs^+ ions (observed from the ion density Table 2) and high Cs^+ residence time is hypothesized to contribute to the longer residence time for NO_3^-.

Ion Induced Perturbations to the Instantaneous Surface and Subjacent Layers

This sections first builds upon prior work that has investigated macroscopic ion induced perturbations to both the vapor and octanol interfaces.[60,67–69] As observed when comparing water/vapor and water/octanol interfaces, within the electrolyte interfaces there exist significant differences in the relationship between γ, d, and ΔA in the presence of octanol. While

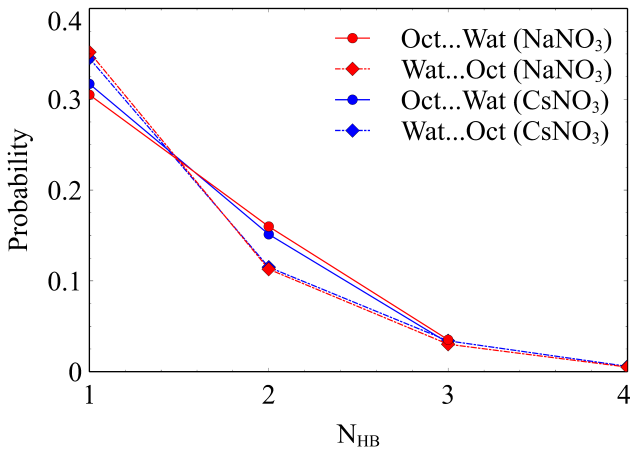

Figure 4: The HB distribution with respect to octanol and water in $NaNO_{3(aq)}$/octanol and $CsNO_{3(aq)}$/octanol syatems.

the water- and electrolyte/vapor biphasic systems all exhibit the expected anticorrelated relationship of γ and d (as interfacial tension increases the interfacial width decreases)—all octanol biphasic systems have a positive correlation of γ and d. When examining the electrolyte containing interfaces, there is an increase to interfacial tension, as anticipated, in the vapor and octanol systems (Table 1). The percent increase is dramatic in the latter case with an average increase of ∼126.24% for $NaNO_{3(aq)}$/octanol and ∼45.95% for $CsNO_{3(aq)}$/octanol when measured in the NPT ensemble. The perturbation by ions upon the fluctuation of the instantaneous surface is more prominent in the octanol biphasic systems, as revealed by studying the trends in in free energies of interfacial deformation (Table 1). For example, $CsNO_{3(aq)}$/octanol interfacial structure is observed to deform ∼1.5 times more easily compared to $CsNO_{3(aq)}$/vapor. The free energy change of 57.9 kJ/mol is primarily due to change in interfacial tension γ.

We then analyze the interfacial organization, from the perspective of water and octanol, the complete H-bonding network of H_2O...H_2O, Oct...Oct, H_2O...Oct and Oct...H_2O was examined. It is well understood that that ion solvation by H_2O decreases H_2O...H_2O H-bonds,[65] and is concentration dependent. Indeed, this is observed in the average decrease in bulk H_2O...H_2O H-bonds by 0.2-0.3 in the 1M electrolyte solution in both the vapor and octanol biphasic systems. Yet this result does not carry over to the interfacial region. In the

electrolyte/vapor system, the presence of the ions (which selectively reside in trough regions), does not significantly impact the H_2O...H_2O HB number. Moving from the water/vapor to water/octanol also does not significantly alter the H_2O...H_2O HB number, yet when ions are introduced a large decrease in HBs is observed. This is in spite of the fact that the impact of ion solvation upon H_2O...H_2O HB should be offset by the fact that octanol replaces a H_2O in the solvation shell of Na^+ and Cs^+. Instead, the change in H_2O...H_2O hydrogen bonding can be attributed to NO_3^--H_2O interactions (Figure 3H). The NO_3^- ions significantly lose water of hydration based upon where they reside in the interfacial region. The loss of ∼0.33 hydrogen bond in crest with addition to electrolyte is predominantly due to an average 0.45 ± 0.06 and 0.39 ± 0.05 H-bond formation by H_{H_2O}-$O_{NO_3^-}$ in $NaNO_{3(aq)}$/octanol and $CsNO_{3(aq)}$/octanol respectively. An average decrease in ∼0.12 hydrogen bond in trough region compared to bulk is also consistent with a 0.14 ± 0.09 and 0.14 ± 0.08 increase in NO_3^--H_2O interactions in both $NaNO_3$ and $CsNO_3$ systems respectively.The effect of ions upon the H_2O...Oct HBs is minor (Figure 4).

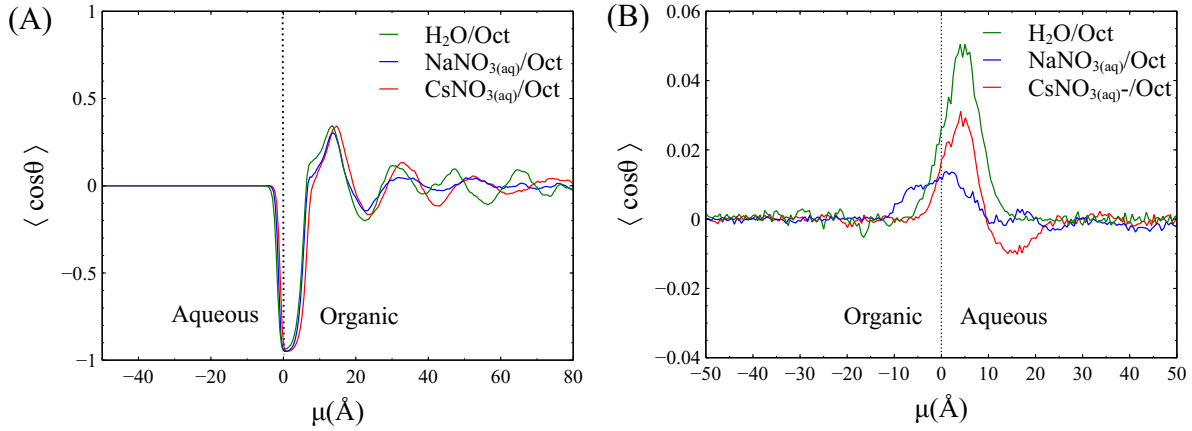

Figure 5: (A) The octanol end-to-end vector orientation profiles with respect to mean position μ in water/octanol(green) $NaNO_{3(aq)}$/octanol(blue) and $CsNO_{3(aq)}$/octanol(red) systems.(B) The net dipole orientation profiles of water molecules of all three water/octanol systems.

Finally, the electrolyte induced perturbations in dipole orientation of water and octanol molecules were examined. Although the presence of ions does little to alter H_2O orientation

at the vapor systems (Figure S9), the dipole orientation of H_2O in the electrolyte/octanol system (Figure 5B) exhibits orientational ordering. Notably, the largest deviations occur far from the interfacial regions we have studied, 10-20 Å from the instantaneous surface, that indicates water becoming less ordered with decreasing cation size from Cs^+ to Na^+. Note, the negative peak between 10-20 Å of $CsNO_3$ system, that is also correlated with a 40% increase in $CsNO_3$ contact ion pair interactions compared to $NaNO_3$. Interestingly, these ion-pair interactions influence the orientation of waters that *are not solvating* the ions,[70] as indicated in the distribution of orientation of H_2O solvating ions and those not having any ion-interactions (Figure S14). Perhaps unsurprisingly, given the small number of ion...Oct interactions, the orientation of octanol is relatively unchanged in the presence of the electrolyte. As in the water/octanol system, the orientation of the octanol end-to-end vector (Figure 5A) favors an orientation perpendicular to the interface, in agreement with prior studies.[71]

Conclusions

The organization and dynamics of water/octanol liquid/liquid interfaces were studied in relation to analogous water/vapor interfaces. In comparison, the pure water/octanol interface was found to be less heterogeneous, as determined from number densities of interfacial molecules and graph theoretical approach to calculate interfacial H_2O-H_2O and H_2O-octanol H-bonding. This fundamental change in interfacial structure is attributable to the strong octanol-water interactions, that subsequently lead to "interdigitation" of the interfacial water and octanol molecules. Interfacial heterogeneity has a large impact upon the distribution of ions within the interfacial region when analogous $NaNO_3$ and $CsNO_3$ electrolyte solutions were examined. Ions at the water/vapor interface were observed to reside primarily in the trough region of capillary waves to avoid loss of solvating water, yet this behavior was diminished in the electrolyte octanol interfaces. An increased ion concentration at the interface

is found to be most highly correlated with the ability of octanol to integrate into the HB network of interfacial solvents—thus preventing significant changes to ion solvation when it resides in the interface. This interplay of competing forces introduced by strong octanol-water interactions provides one mechanism for altering ion concentration and potentially reactivity at the interface.

Acknowledgements

This work was supported by a grant from Department of Energy, Basic Energy Sciences Separations program (DE-SC0001815). N.K. acknowledges the PNNL-WSU Distinguished Graduate Research Program for tuition waivers. This research used resources from the Center for Institutional Research Computing at Washington State University.

References

(1) Chang, T.-M.; Dang, L. X. Recent Advances in Molecular Simulations of Ion Solvation at Liquid Interfaces. *Chemical Reviews* **2006**, *106*, 1305–1322.

(2) Benjamin, I. Molecular Structure and Dynamics at Liquid–Liquid Interfaces. *Annual review of physical chemistry* **1997**, *48*, 407–451.

(3) Jungwirth, P.; Winter, B. Ions at Aqueous Interfaces: From Water Surface to Hydrated Proteins. *Annual Review of Physical Chemistry* **2008**, *59*, 343–366.

(4) Luo, G.; Malkova, S.; Yoon, J.; Schultz, D. G.; Lin, B.; Meron, M.; Benjamin, I.; Vanýsek, P.; Schlossman, M. L. Ion Distributions Near a Liquid-Liquid Interface. *Science* **2006**, *311*, 216–218.

(5) Liang, Z.; Bu, W.; Schweighofer, K. J.; Walwark, D. J.; Harvey, J. S.; Hanlon, G. R.; Amoanu, D.; Erol, C.; Benjamin, I.; Schlossman, M. L. Nanoscale View of Assisted Ion

Transport Across the Liquid–Liquid Interface. *Proceedings of the National Academy of Sciences* **2019**, *116*, 18227–18232.

(6) Mitrinovic, D. M.; Zhang, Z.; Williams, S. M.; Huang, Z.; Schlossman, M. L. X-Ray Reflectivity Study of the Water-Hexane Interface. *The Journal of Physical Chemistry B* **1999**, *103*, 1779–1782.

(7) Zhang, Y.; Feller, S. E.; Brooks, B. R.; Pastor, R. W. Computer Simulation of Liquid/Liquid Interfaces : Theory and Application to Octane/Water. *The Journal of chemical physics* **1995**, *103*, 10252–10266.

(8) MacKerell Jr, A. D.; Bashford, D.; Bellott, M.; Dunbrack Jr, R. L.; Evanseck, J. D.; Field, M. J.; Fischer, S.; Gao, J.; Guo, H.; Ha, S. et al. All-Atom Empirical Potential for Molecular Modeling and Dynamics Studies of Proteins. *The journal of physical chemistry B* **1998**, *102*, 3586–3616.

(9) Lazaridis, T.; Karplus, M. Effective Energy Function for Proteins in Solution. *Proteins: Structure, Function, and Bioinformatics* **1999**, *35*, 133–152.

(10) Zhou, T.; McCue, A.; Ghadar, Y.; Bakó, I.; Clark, A. E. Structural and Dynamic Heterogeneity of Capillary Wave Fronts at Aqueous Interfaces. *The Journal of Physical Chemistry B* **2017**, *121*, 9052–9062.

(11) Jungwirth, P.; Tobias, D. J. Molecular Structure of Salt Solutions : A New View of the Interface with Implications for Heterogeneous Atmospheric Chemistry. *The Journal of Physical Chemistry B* **2001**, *105*, 10468–10472.

(12) Thomas, J. L.; Roeselová, M.; Dang, L. X.; Tobias, D. J. Molecular Dynamics Simulations of the Solution Air Interface of Aqueous Sodium Nitrate. *The Journal of Physical Chemistry A* **2007**, *111*, 3091–3098.

(13) Petersen, P. B.; Saykally, R. J. On the Nature of Ions at the Liquid Water Surface. *Annual Review of Physical Chemistry* **2006**, *57*, 333–364.

(14) Collins, K. D.; Washabaugh, M. W. The Hofmeister Effect and the Behaviour of Water at Interfaces. *Quarterly reviews of biophysics* **1985**, *18*, 323–422.

(15) Cacace, M.; Landau, E.; Ramsden, J. The Hofmeister Series: Salt and Solvent Effects on Interfacial Phenomena. *Quarterly reviews of biophysics* **1997**, *30*, 241–277.

(16) Servis, M. J.; Clark, A. E. Surfactant-Enhanced Heterogeneity of the Aqueous Interface Drives Water Extraction into Organic Solvents. *Physical Chemistry Chemical Physics* **2019**, *21*, 2866–2874.

(17) Chorny, I.; Benjamin, I. Hydration Shell Exchange Dynamics during Ion Transfer across the Liquid/Liquid Interface. *The Journal of Physical Chemistry B* **2005**, *109*, 16455–16462.

(18) Otten, D. E.; Shaffer, P. R.; Geissler, P. L.; Saykally, R. J. Elucidating the Mechanism of Selective Ion Adsorption to the Liquid Water Surface. *Proceedings of the National Academy of Sciences* **2012**, *109*, 701–705.

(19) Venkateshwaran, V.; Vembanur, S.; Garde, S. Water-Mediated Ion–Ion Interactions are Enhanced at the Water Wapor–Liquid Interface. *Proceedings of the National Academy of Sciences* **2014**, *111*, 8729–8734.

(20) Wang, Y.; Sinha, S.; Desai, P. R.; Jing, H.; Das, S. Ion at Air-Water Interface Enhances Capillary Wave Fluctuations: Energetics of Ion Adsorption. *Journal of the American Chemical Society* **2018**, *140*, 12853–12861.

(21) Abraham, M. J.; Murtola, T.; Schulz, R.; Páll, S.; Smith, J. C.; Hess, B.; Lindahl, E. GROMACS: High Performance Molecular Simulations Through Multi-Level Parallelism from Laptops to Supercomputers. *SoftwareX* **2015**, *1*, 19–25.

(22) Martínez, L.; Andrade, R.; Birgin, E. G.; Martínez, J. M. PACKMOL: A Package for Building Initial Configurations for Molecular Dynamics Simulations. *Journal of computational chemistry* **2009**, *30*, 2157–2164.

(23) Darden, T.; York, D.; Pedersen, L. Particle Mesh Ewald: An N log (N) Method for Ewald Sums in Large Systems. *The Journal of chemical physics* **1993**, *98*, 10089–10092.

(24) Neria, E.; Fischer, S.; Karplus, M. Simulation of Activation Free Energies in Molecular Systems. *The Journal of chemical physics* **1996**, *105*, 1902–1921.

(25) Joung, I. S.; Cheatham III, T. E. Determination of Alkali and Halide Monovalent Ion Parameters for use in Explicitly Solvated Biomolecular Simulations. *The journal of physical chemistry B* **2008**, *112*, 9020–9041.

(26) Megyes, T.; Bálint, S.; Peter, E.; Grósz, T.; Bakó, I.; Krienke, H.; Bellissent-Funel, M.-C. Solution Structure of NaNO3 in Water: Diffraction and Molecular Dynamics Simulation Study. *The Journal of Physical Chemistry B* **2009**, *113*, 4054–4064.

(27) Tongraar, A.; Liedl, K. R.; , B. M. Born- Oppenheimer Ab Initio QM/MM Dynamics Simulations of Na+ and K+ in Water: From Structure Making to Structure Breaking Effects. *The Journal of Physical Chemistry A* **1998**, *102*, 10340–10347.

(28) White, J. A.; Schwegler, E.; Galli, G.; Gygi, F. The Solvation of Na+ in Water: First-Principles Simulations. *The Journal of Chemical Physics* **2000**, *113*, 4668–4673.

(29) Schwenk, C. F.; Hofer, T. S.; , B. M. "Structure Breaking" Effect of Hydrated Cs+. *The Journal of Physical Chemistry A* **2004**, *108*, 1509–1514.

(30) Baaden, M.; Burgard, M.; Wipff, G. TBP at the Water- Oil Interface: The Effect of TBP Concentration and Water Acidity Investigated by Molecular Dynamics Simulations. *The Journal of Physical Chemistry B* **2001**, *105*, 11131–11141.

(31) Guilbaud, P.; Wipff, G. Hydration of Uranyl Cation and its Nitrate Ion and 18-Crown-6 Adducts Studied by Molecular Dynamics Simulations. *The Journal of Physical Chemistry* **1993**, *97*, 5685–5692.

(32) Papoyan, G.; Gu, K.-j.; Wiorkiewicz-Kuczera, J.; Kuczera, K.; Bowman-James, K. Molecular Dynamics Simulations of Nitrate Complexes with Polyammonium Macrocycles: Insight on Phosphoryl Transfer Catalysis. *Journal of the American Chemical Society* **1996**, *118*, 1354–1364.

(33) Smith, J. W.; Lam, R. K.; Shih, O.; Rizzuto, A. M.; Prendergast, D.; Saykally, R. J. Properties of Aqueous Nitrate and Nitrite from X-Ray Absorption Spectroscopy. *The Journal of chemical physics* **2015**, *143*, 084503.

(34) Mark, P.; Nilsson, L. Structure and Dynamics of the TIP3P, SPC, and SPC/E Water Models at 298 K. *The Journal of Physical Chemistry A* **2001**, *105*, 9954–9960.

(35) Horn, H. W.; Swope, W. C.; Pitera, J. W.; Madura, J. D.; Dick, T. J.; Hura, G. L.; Head-Gordon, T. Development of an Improved Four-Site Water Model for Biomolecular Simulations: TIP4P-Ew. *The Journal of chemical physics* **2004**, *120*, 9665–9678.

(36) Vega, C.; De Miguel, E. Surface Tension of the Most Popular Models of Water by Using the Test-Area Simulation Method. *The Journal of chemical physics* **2007**, *126*, 154707.

(37) Taylor, R. S.; Dang, L. X.; Garrett, B. C. Molecular Dynamics Simulations of the Liquid/Vapor Interface of SPC/E Water. *The Journal of Physical Chemistry* **1996**, *100*, 11720–11725.

(38) Jorgensen, W. L.; Maxwell, D. S.; Tirado-Rives, J. Development and Testing of the OPLS All-Atom Force Field on Conformational Energetics and Properties of Organic Liquids. *Journal of the American Chemical Society* **1996**, *118*, 11225–11236.

(39) Alejandre, J.; Tildesley, D. J.; Chapela, G. A. Molecular Dynamics Simulation of the Orthobaric Densities and Surface Tension of Water. *The Journal of chemical physics* **1995**, *102*, 4574–4583.

(40) Wick, C. D.; Chang, T.-M. Computational Observation of Pockets of Enhanced Water Concentration at the 1-Octanol/Water Interface. *The Journal of Physical Chemistry B* **2014**, *118*, 7785–7791.

(41) Napoleon, R. L.; Moore, P. B. Structural Characterization of Interfacial n-Octanol and 3-Octanol using Molecular Dynamic Simulations. *The Journal of Physical Chemistry B* **2006**, *110*, 3666–3673.

(42) Hantal, G.; Darvas, M.; Partay, L. B.; Horvai, G.; Jedlovszky, P. Molecular Level Properties of the Free Water Surface and Different Organic Liquid/Water Interfaces, as Seen from ITIM Analysis of Computer Simulation Results. *Journal of Physics: Condensed Matter* **2010**, *22*, 284112.

(43) Sega, M.; Fábián, B.; Jedlovszky, P. Layer-by-Layer and Intrinsic Analysis of Molecular and Thermodynamic Properties Across Soft Interfaces. *The Journal of chemical physics* **2015**, *143*, 114709.

(44) Ozkanlar, A.; Clark, A. E. ChemNetworks: A Complex Network Analysis Tool for Chemical Systems. *Journal of computational chemistry* **2014**, *35*, 495–505.

(45) Berberan-Santos, M.; Bodunov, E.; Valeur, B. Mathematical Functions for the Analysis of Luminescence Decays with Underlying Distributions 1. Kohlrausch Decay Function (Stretched Exponential). *Chemical Physics* **2005**, *315*, 171–182.

(46) Lísal, M.; Posel, Z.; Izák, P. Air–Liquid Interfaces of Imidazolium-Based [TF 2 N-] Ionic Liquids: Insight from Molecular Dynamics Simulations. *Physical Chemistry Chemical Physics* **2012**, *14*, 5164–5177.

(47) Willard, A. P.; Chandler, D. Instantaneous Liquid Interfaces. *The Journal of Physical Chemistry B* **2010**, *114*, 1954–1958.

(48) Liu, Z.; Stecher, T.; Oberhofer, H.; Reuter, K.; Scheurer, C. Response Properties at the Dynamic Water/Dichloroethane liquid–liquid interface. *Molecular Physics* **2018**, *116*, 3409–3416.

(49) Dang, L. X. Computational Study of Ion Binding to the Liquid Interface of Water. *The Journal of Physical Chemistry B* **2002**, *106*, 10388–10394.

(50) Benjamin, I. Mechanism and Dynamics of Ion Transfer Across a Liquid-Liquid interface. *Science* **1993**, 1558–1560.

(51) Ghadar, Y.; Christensen, S. L.; Clark, A. E. Influence of Aqueous Ionic Strength Upon Liquid:Liquid Interfacial Structure and Microsolvation. *Fluid Phase Equilibria* **2016**, *407*, 126 – 134, Aqueous Solutions.

(52) Demond, A. H.; Lindner, A. S. Estimation of Interfacial Tension Between Organic Liquids and Water. *Environmental science & technology* **1993**, *27*, 2318–2331.

(53) Chen, F.; Smith, P. Simulated Surface Tensions of Common Water Models. *The Journal of chemical physics* **2007**, *126*, 221101–221101.

(54) DasGupta, S.; Schonberg, J. A.; Kim, I. Y.; Wayner Jr, P. C. Use of the augmented Young-Laplace equation to model equilibrium and evaporating extended menisci. *Journal of colloid and interface science* **1993**, *157*, 332–342.

(55) Oostenbrink, C.; Villa, A.; Mark, A. E.; Van Gunsteren, W. F. A Biomolecular Force Field Based on the Free Enthalpy of Hydration and Solvation: The GROMOS Force-Field Parameter Sets 53A5 and 53A6. *Journal of computational chemistry* **2004**, *25*, 1656–1676.

(56) Aveyard, R.; Saleem, S. M. Interfacial Tensions at Alkane-Aqueous Electrolyte Interfaces. *Journal of the Chemical Society, Faraday Transactions 1: Physical Chemistry in Condensed Phases* **1976**, *72*, 1609–1617.

(57) Minofar, B.; Vácha, R.; Wahab, A.; Mahiuddin, S.; Kunz, W.; Jungwirth, P. Propensity for the Air/Water Interface and Ion Pairing in Magnesium Acetate vs Magnesium Nitrate solutions: Molecular dynamics simulations and surface tension measurements. *The Journal of Physical Chemistry B* **2006**, *110*, 15939–15944.

(58) McFearin, C. L.; Richmond, G. L. The Role of Interfacial Molecular Structure in the Adsorption of Ions at the Liquid-Liquid Interface. *The Journal of Physical Chemistry C* **2009**, *113*, 21162–21168.

(59) Jarvis, N. L.; Scheiman, M. A. Surface Potentials of Aqueous Electrolyte Solutions. *The Journal of Physical Chemistry* **1968**, *72*, 74–78.

(60) Tesei, G.; Aspelin, V.; Lund, M. Specific Cation Effects on SCN–in Bulk Solution and at the Air–Water Interface. *The Journal of Physical Chemistry B* **2018**, *122*, 5094–5105.

(61) Pegram, L. M.; Record, M. T. Hofmeister Salt Effects on Surface Tension Arise from Partitioning of Anions and Cations Between Bulk Water and the Air- Water Interface. *The journal of physical chemistry B* **2007**, *111*, 5411–5417.

(62) Brown, M. A.; D'Auria, R.; Kuo, I.-F. W.; Krisch, M. J.; Starr, D. E.; Bluhm, H.; Tobias, D. J.; Hemminger, J. C. Ion Spatial Distributions at the Liquid–Vapor Interface of Aqueous Potassium Fluoride Solutions. *Physical Chemistry Chemical Physics* **2008**, *10*, 4778–4784.

(63) Hribar, B.; Southall, N. T.; Vlachy, V.; Dill, K. A. How Ions Affect the Structure of Water. *Journal of the American Chemical Society* **2002**, *124*, 12302–12311.

(64) Baer, M. D.; Mundy, C. J. Toward an Understanding of the Specific Ion effect Using Density Functional Theory. *The Journal of Physical Chemistry Letters* **2011**, *2*, 1088–1093.

(65) Rock, W.; Qiao, B.; Zhou, T.; Clark, A. E.; Uysal, A. Heavy Anionic Complex Creates a Unique Water Structure at a Soft Charged Interface. *The Journal of Physical Chemistry C* **2018**, *122*, 29228–29236.

(66) Phan, C. M. Dynamic Adsorption of Octanols at Air/Water Interface. *The Canadian journal of chemical engineering* **2010**, *88*, 688–692.

(67) Mucha, M.; Frigato, T.; Levering, L.; Allen, H.; Tobias, D.; Dang, L.; Jungwirth, P. Unified Molecular Picture of the Surfaces of Aqueous Acid, Base, and Salt Solutions. *The journal of physical chemistry. B* **2005**, *109*, 7617–7623.

(68) Caleman, C.; Hub, J. S.; van Maaren, P. J.; van der Spoel, D. Atomistic Simulation of Ion Solvation in Water Explains Surface Preference of Halides. *Proceedings of the National Academy of Sciences* **2011**, *108*, 6838–6842.

(69) Bastos-Gonzalez, D.; Perez-Fuentes, L.; Drummond, C.; Faraudo, J. Ions at Interfaces: The Central Role of Hydration and Hydrophobicity. *Current opinion in colloid & interface science* **2016**, *23*, 19–28.

(70) Stirnemann, G.; Wernersson, E.; Jungwirth, P.; Laage, D. Mechanisms of Acceleration and Retardation of Water Dynamics by Ions. *Journal of the American Chemical Society* **2013**, *135*, 11824–11831.

(71) Benjamin, I. Polarity of the Water/Octanol Interface. *Chemical physics letters* **2004**, *393*, 453–456.

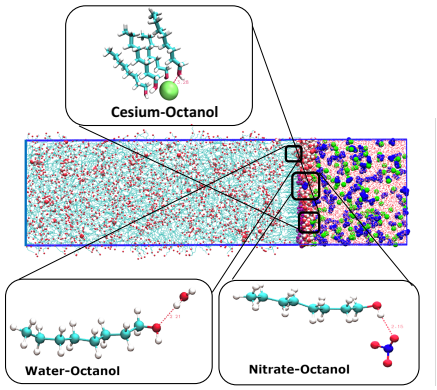

Figure 6: This is a TOC image.